Experimental investigation on the physical parameters of ionic polymer metal composites sensors for humidity perception

Yanjie Wang[a,1]*, Gangqiang Tang[a,1], Chun Zhao[a], Keli Wang[b], Jiale Wang[c], Jie Ru[a], Junjie Sheng[d]*, Longfei Chang[e], Lijie Li[f]

[a] *Jiangsu Provincial Key Laboratory of Special Robot Technology, Hohai University, Changzhou campus, Changzhou, 213022, China*

[b] *School of Mechanical Engineering and Automation, Beihang University, Beijing 100191, People's Republic of China*

[c] *Department of Astronautical Science and Mechanics, Harbin Institute of Technology, Harbin, 150006, China.*

[d] *Institute of Systems Engineering, China Academy of Engineering Physics, Mianyang, 1111, China*

[e] *Anhui Province Key Lab of Aerospace Structural Parts Forming Technology and Equipment, Hefei University of Technology, Hefei, 230009, China*

[f] *College of Engineering, Swansea University, Swansea, SA1 8EN, UK*

* Corresponding authors: Yanjie Wang and Junjie Sheng

Email: yj.wang1985@gmail.com and scu2005sjj@163.com

[1] The two authors contributed equally: Yanjie Wang, Gangqiang Tang.

Abstract

Ionic polymer metal composite (IPMC) is one of typical electromechanical transducing materials integrating actuation and sensing functions. In this work, we systematically investigate the evolution of the capacitance, surface resistance and ionic electrical response of strip shaped IPMC under different humidity conditions. For each parameter, we have performed a set of static and dynamic humidity sensing tests, considering the change of the thickness, cations and impregnation-reduction plating (IRP) times. Through conducting a series of experiments, it is concluded that the humidity-capacitance sensing has achieved a much wider sensing range (22% RH - 100%RH in this work, comparing with 40% RH - 90%RH in previous work) and an increased sensitivity (256μF in this work, comparing with140nF in previous work). In the meantime, humidity-surface resistance sensing has the perception of the full humidity range. While the humidity-ionic electrical response sensing can only respond to dynamic humidity changes but showing a very fast response time of less than 0.5 s, which will be of great significance in some special humidity detection scenarios, such as the rapid detection and alarm of leakage of equipment with constant humidity. For each case, it implies a fact that the water absorption capacity of surface electrode and inter layer determines the humidity sensing abilities, such as response speed, amplitude and so on.

Key words: IPMC, humidity sensing, capacitance, surface resistance, ionic electrical response

1 Introduction

Ionic polymer metal composite (IPMC) is one type of electroactive materials with excellent sensing and actuation ability, which has been widely used as actuators and sensors (deformation, pressure, humidity and so on) in the field of bionics [1-4]. IPMC typically consists of a sheet of electrically activated polymer (usually Nafion, Flemion and Aciplex) sandwiched by two conductive electrodes. Inside the polymer, the anions covalently bound to the polymer chain are balanced with movable cations, which can migrate through the nano-ion channels [5, 6]. In terms of actuation, when applying a voltage to the electrodes, cations move rapidly under the action of electric field. IPMC bends sharply due to uneven pressure gradient, presenting two advantages of high curvature and high sensitivity [7, 8]. In terms of sensing, IPMC has inherent sensing characteristics because of the redistributed cations in response to uneven stress and ion concentration [9, 10]. When IPMC bends, cations migrate under the action of pressure gradient, so a perceptive electrical signal can be measured between the electrodes, which can be used to measure the deformation of IPMC [11, 12]. When a mechanical force is applied to IPMC, ion migration will generate electrical signals due to directional pressure, which can be used to measure the applied pressure of IPMC [13-15]. Based on the above mechanisms, IPMC can be utilized as deformation and pressure sensors. Meanwhile, due to the water swelling and ion selective permeability of inter-layer, the physical parameters of IPMC, such as capacitance, surface resistance and ionic distribution, will definitely change so that IPMC can also be potentially used for humidity sensors.

In fact, humidity was firstly studied as an influencing factor of the electromechanical behavior of IPMC. *Junho Li* et al. researched the water uptake and migration effects of IPMC actuator in 2005 [16]. In 2007, *Eiichi Shoji* et al. studied the effects of humidity on the performance of IPMC actuators [17] and in 2011, *Paola Brunetto* et al. characterized the temperature and humidity influence on IPMC as sensors [18]. In 2016, *Zicai Zhu* et al. found that the environmental humidity has a great influence on the bending deformation sensing signal of IPMC [19, 20]. Based on the influence of humidity on the actuating behavior, *Jie Ru* et al. proposed a mechanism that used the coupling of humidity and electrical signal to control IPMC actuation in 2018 [21]. The previous studies showed that IPMC is sensitive to water molecular and has the potential to be developed into a humidity sensor. Meanwhile, the work of using IPMC in humidity sensing began in 2017, *Emad Esmaeli et al.* used Ti and Cr as the adhesion layer between Nafion and Au electrodes to prepare IPMC samples and its capacitance value was measured under different static humidity environment [22]. Subsequently, *Fahimeh Beigi* et al. performed an improved study on IPMC humidity sensing in 2018 that they prepared IPMC with Nafion membrane doped with layered double hydroxide (LDH) nanoparticles to increase the water absorption of IPMC and studied its ionic electrical response to humidity [23].

In previous works, researchers mainly focus on the response of single parameter of IPMC to humidity. In fact, IPMC consists of one ionomer and two electrode layers. The ionomer acts a key role on humidity sensing ability of IPMC. The internal composition of the ionomer includes two-phase microstructure (solid-liquid), which

represents agglomerate molecular long chain and ionic solvent region, respectively, and the end of the long chain has hydrophilic sulfonic acid group, which can bond cations together with several water molecules. Therefore, the ionomer has intrinsic water swelling, ion migration and other characteristics, which results in multi-parameter responses under the effect of humidity. As a stable commercial ion exchange membrane with high hygroscopicity and ion selectivity, Nafion is the most commonly used humidity sensitive ionomer [24-26]. In this work, we employed the Nafion film as an interlayer of IPMC. As shown in Fig. 1, after absorbing water, the physical properties of IPMC show obvious uneven swelling changes. Firstly, the swelling of Nafion layer after absorbing water leads to the change of the capacitance of the double layer. It indicates that this material can be potentially used as a capacitance-humidity sensor. Secondly, due to the loose characteristics of the surface electrode, the resistance of the electrode layer increases accordingly together with the volume change caused by IPMC water absorption, with which IPMC can be potentially used as a resistance-humidity sensor. Finally, internal ions migrate in a directional way under the action of uneven swelling of IPMC, and ionic electrical response can be detected between the electrode layers. It means that IPMC can be potentially used as a voltage-humidity sensor.

In this work, it is the first time to comprehensively study the responses of various physical parameters of IPMC under the humidity effect. It will be helpful to distinguish the advantages of each mechanism, and to select a relatively suitable sensing mechanism in a specific application. We investigated the effects of humidity

on the capacitance, surface resistance and ionic electrical response of IPMC, and the factors affecting its humidity sensing performance were discussed and clarified, such as the thickness of interlayer and electrode layer and cations type.

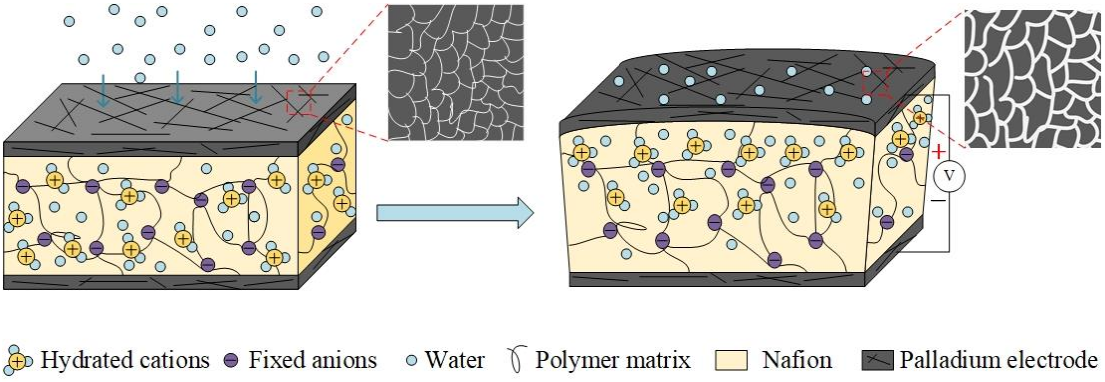

Fig. 1. Mechanism of IPMC humidity sensing

2 Experimental Section

2.1 Preparation of IPMC

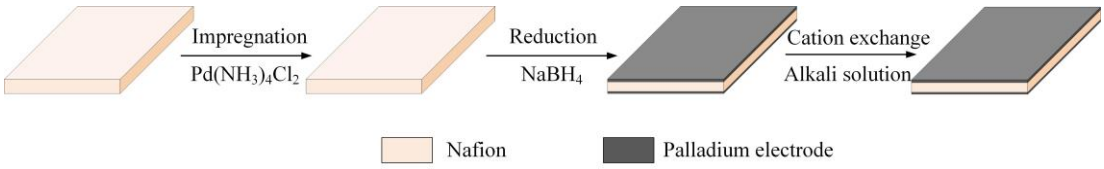

Fig. 2. The preparation process of IPMC

In this experiment, Nafion117 is used as the interlayer, which was purchased from Dupont, USA. Auxiliary reagents such as $Pd(NH_3)_4Cl_2$, $NaBH_4$, and HCl were obtained from J&K Chemical Inc.(Beijing, China). The preparation process is shown in Fig. 2. The preparation process used in this work is different from the traditional process that only impregnation-reduction plating is used, considering the balance of conductivity and water absorption. The detailed preparation process is described as follows.

(a) Pretreatment. The matrix film of a certain size was cut and cleaned by ultrasonic in deionized (DI) water for 30 min (50℃). Then the film was immersed in HCL at 2 mol/L (99℃) and DI water (99℃) for 30 min. The purpose of this process is to remove the impurity on the substrate surface.

(b) Impregnation-reduction plating (IRP). The pre-treated membrane was placed in an ammonia solution of $Pd(NH_3)_4Cl_2$ at 0.01 mol/L, heated and oscillated in a water bath thermostatic oscillator for 60 min (50℃, 90 r/min). After rinsed with DI water, the film was soaked in ammonia solution of $NaBH_4$ at 0.02 mol/L and heated for another 30 min (50℃, 90 r/min). The process is to replace the palladium ions in the palladium complex into the polymer and to reduce the palladium ions to palladium particles on the surface of the matrix film. Sample with more IRP times can be prepared by repeating this step.

(c) Post-treatment. The sample was trimmed after IRP step, then soaked in 0.2 mol/L alkali solution (LiOH, NaOH, KOH) for 2 h, and finally put in DI water for standby use. The purpose of this step is to conduct cation (Li^+, Na^+, K^+) exchange.

Table 1. The parameters of IPMC samples

Number	Thickness (mm)	Cation type	IRP times
A	0.05	Na^+	1
B	0.1	Na^+	1
C	0.2	Na^+	1
D	0.05	Li^+	1
E	0.05	K^+	1
F	0.05	Na^+	2
G	0.05	Na^+	3

After the preparation, all the samples were cut into sheets with the size of 5 mm×25 mm. The surface images of sample A, F and G observed by a metallurgical

microscope are shown in Fig. 3. It is worth noting that the color temperature and white balance of each image are different due to the difference in the surface sensitivity. According to the experiment design scheme, the samples used in our experiments are numbered and listed in Table 1. By comparing sample A, B and C, the influence of thickness on IPMC humidity sensing can be clarified. By comparing sample A, D and E, the influence of cation types was analyzed and discussed together with the influence of IRP times by comparing sample A, F and G.

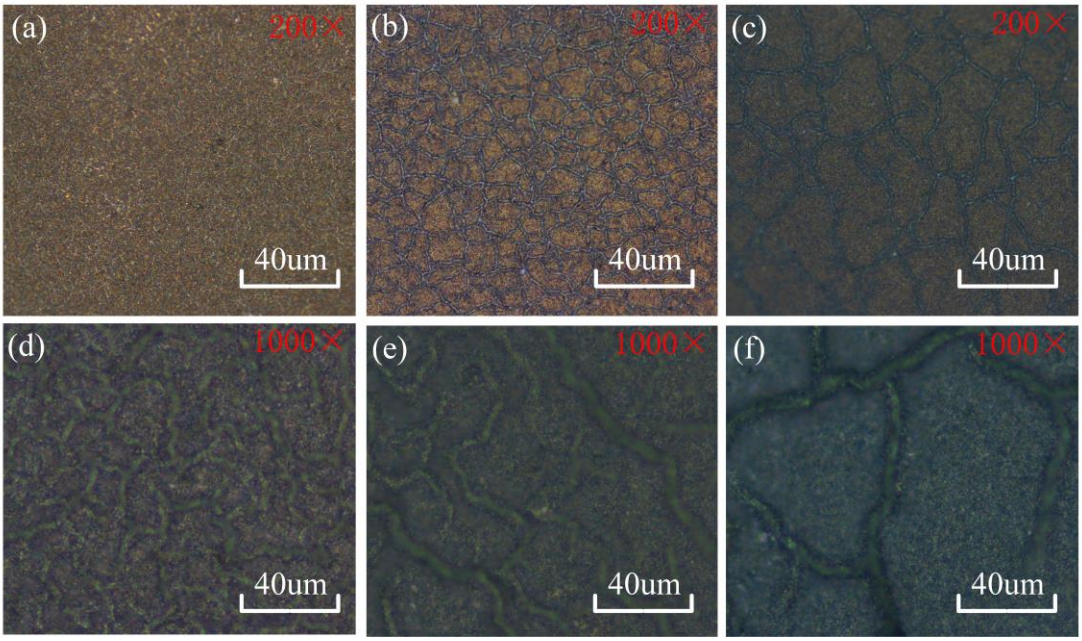

Fig. 3. Metallurgical microscope image of different samples. (a) 200 times magnification of the surface of sample A. (b) 200 times magnification of the surface of sample F. (c) 200 times magnification of the surface of sample G. (d) 1000 times magnification of the surface of sample A. (e) 1000 times magnification of the surface of sample F. (f) 1000 times magnification of the surface of sample G.

2.2 Method and characterization

2.2.1 Characterization of capacitance and surface resistance responses

According to the aforementioned in section 1, the capacitance and surface resistance of IPMC will change with varying humidity because of the swelling characteristics of the inter-layer after water absorption, it might have a certain corresponding relationship between them. We set up a static test platform to measure the capacitance and surface resistance of IPMC at a fixed humidity, which is composed of a PC, a multimeter with a PC interface channel and static humidity environment. The saturated salt solutions were used to obtain stable relative humidity environment, which is considered to be a more convenient method with high reliability by far. In 1976, *Lewis Greenspan* measured 28 saturated salt solutions and gave the results of an experiment to balance relative humidity and temperature [27]. From *Lewis*'s experimental results, we selected 7 readily available saturated salt solutions to create different relative humidity environments. In addition, a humidity level that is close to 0% RH was obtained by placing excess allochroic silicagel in a confined space, which is a commonly used desiccant that absorbs almost all the moisture in the confined space. A humidity level of almost 100% RH was obtained by placing pure water in a confined space. All humidity environments need to be set for over 12 h to stabilize the humidity. The relative humidity levels of the nine environments at room temperature (25℃) were shown in Table 2.

Table 2. Relative humidity of each environment at room temperature(25℃)

Type of salts	Allochroic silicagel		LiCl	CH_3COOK	$MgCl_2$
RH(%)	Close to 0		11	22	33
Type of salts	K_2CO_3	NaBr	NaCl	KCl	Pure water

RH(%)	43	57	75	84	Close to 100

The measuring process is shown in Fig. 4 (a). IPMC sample was clamped by a fixture and placed in a humidity bottle containing saturated salt solution. The bottle was sealed with PE film and there was no contact between the liquid and IPMC. The parameters of the sample to be measured of the sample were obtained by a VICTOR 86E multimeter and recorded in the PC in real time. As shown in Fig. 4 (b), the fixture was hollow frame on one side and solid plate on the other side to ensure that only one side of IPMC sample can perform humidity exchange with the humidity environment eliminating the influence caused by uneven moisture absorption on both sides. The moisture absorption area on one side of the sample was 5 mm×18 mm. Before each test, the humidity bottle should be sealed and set for over 12 h at room temperature to stabilize the humidity in the bottle. Each measuring time should be kept above 4 h to allow the sample fully conducting humidity exchange at the given humidity level.

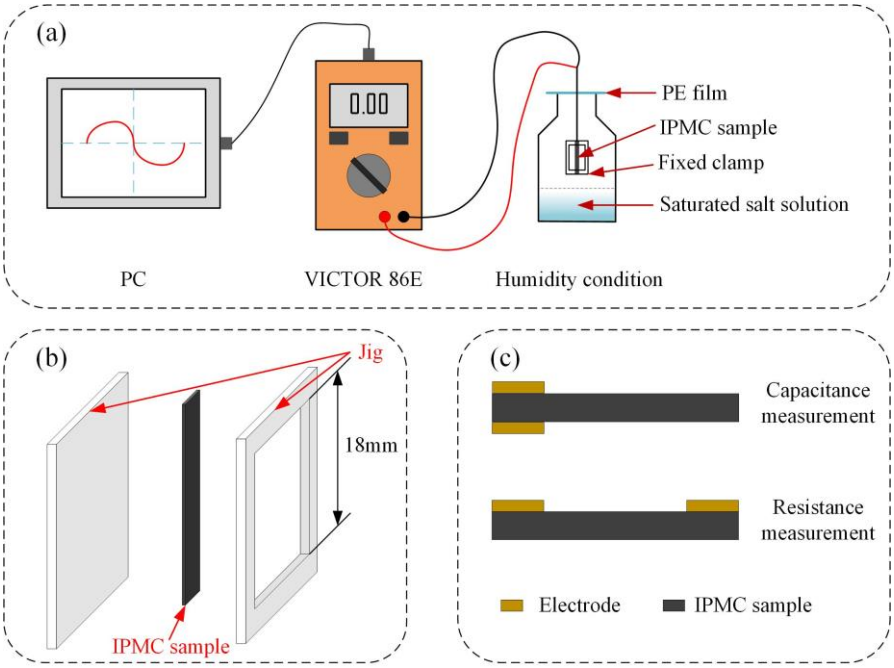

Fig. 4. Capacitance and resistance measuring platform. (a) The measuring progress of

capacitance and resistance. (b) The structure of the jig. (c) The electrode arrangement of the connections during capacitance and resistance measurement.

As shown in Fig. 4 (c), the static measuring platform is suitable for both capacitance measurement and surface resistance measurement. The only difference between them is the electrode arrangement of the connections. For capacitance measurement, electrodes are arranged on both sides of the sample, while electrodes are arranged on both ends of the same side of the sample for surface resistance measurement. Therefore, it is necessary to change the fixture when measuring parameters are switched.

2.2.2 Characterization of ionic electrical response

According to the humidity sensing mechanism of IPMC, an electrical signal can be detected between two electrodes after ion migration caused by water absorption. Different from capacitance and surface resistance, after IPMC fully exchanges at a fixed humidity, its internal ions will no longer migrate, and the stabilized voltage value will gradually approach to 0 V in theory. Subsequently, we performed the dynamic humidity test where four gradients of relative humidity (57%-0%, 57%-43%, 57%-84%, and 57%-100%) were set to explore the dynamic ionic electrical response of IPMC from 57% RH to another humidity level.

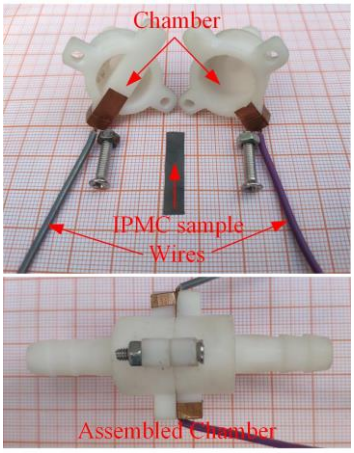

Fig. 5. The mini-chamber for the humidity test

In order to achieve quick humidity switch, a mini-chamber with an inner length of 20 mm and an inner diameter of 18 mm was produced by 3D printing technology. As shown in Fig. 5, the chamber is composed of two similar parts, one of which is equipped with a beam structure. The IPMC sample was placed close to the beam and can be clamped by the other part. In addition to preventing the deformation of the sample under the action of airflow, the beam structure can also ensure that only one side of the sample exchanges water with humidity environment. Because of the small size inside the mini-chamber, it is easy to switch from one humidity environment to another.

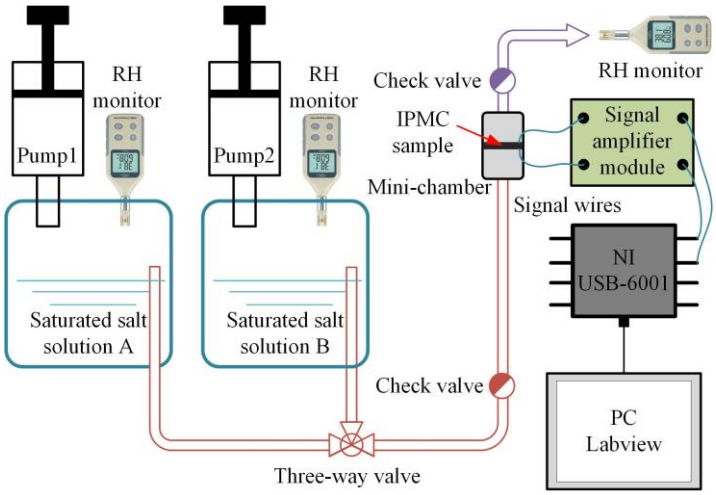

Fig. 6. Ionic electrical measuring platform

The ionic electrical measurement platform is shown in Fig. 6. Saturated salt solution was filled into two humidity tanks A and B. Tank A was filled with saturated NaBr solution to achieve a stable humidity of 57% RH, and different humidity gradients were achieved by changing the humidity gas in tank B. Tank A and tank B are connected to two ends of a three-way valve by pipes, the other end of which is connected to the mini-chamber. In order to prevent backward flow, two check valves are set at the front and rear ends of the cavity. During measurement, air pump 1 was started first and the gas in tank A with relative humidity of 57% RH was pumped into the chamber. It wss ensured that IPMC contacts with gas A for several hours until its voltage response value is stable. Then the three-way valve was adjusted to pump the gas in tank B into the chamber. Due to the instantaneous switch of humidity, ionic electrical response will be detected between two sides of the sample. The entire voltage data was recorded on LABVIEW platform of PC via a data acquisition card of NI USB-6001. Due to the small magnitude of the generated electrical signals, a signal amplifier module was set up ahead of acquisition, and the generated electrical signals were amplified by 50 times. In order to ensure the reliability of the humidity in the chamber, three RH monitors were placed in the humidity tanks and the final exit to detect the humidity level of the gas into and out of the chamber in real time.

3 Results and Discussion

3.1 Water absorption and desorption characteristics

In order to understand the humidity response characteristics of IPMC, the investigations on the water absorption and desorption characteristics of different samples were carried out first. For the absorption process, IPMC sample were heated in a vacuum drying oven at 80℃ for 12 h (named full dry state) and then it was placed in the room humidity (40% RH) condition. For the desorption process, the samples were soaked in DI water for more than 12 h (named full wet state) and placed in room humidity (40% RH) condition after wiping off the surface water with wet filter paper. The mass of IPMC was detected by an electronic balance during the two progresses. The mass in full dry state is defined as m_{dry}, and the real-time mass in the process of water loss and water absorption is defined as m, the water content is defined as W, then the real-time water content calculation formula can be expressed as follow:

$$W = \frac{m - m_{dry}}{m_{dry}} \tag{1}$$

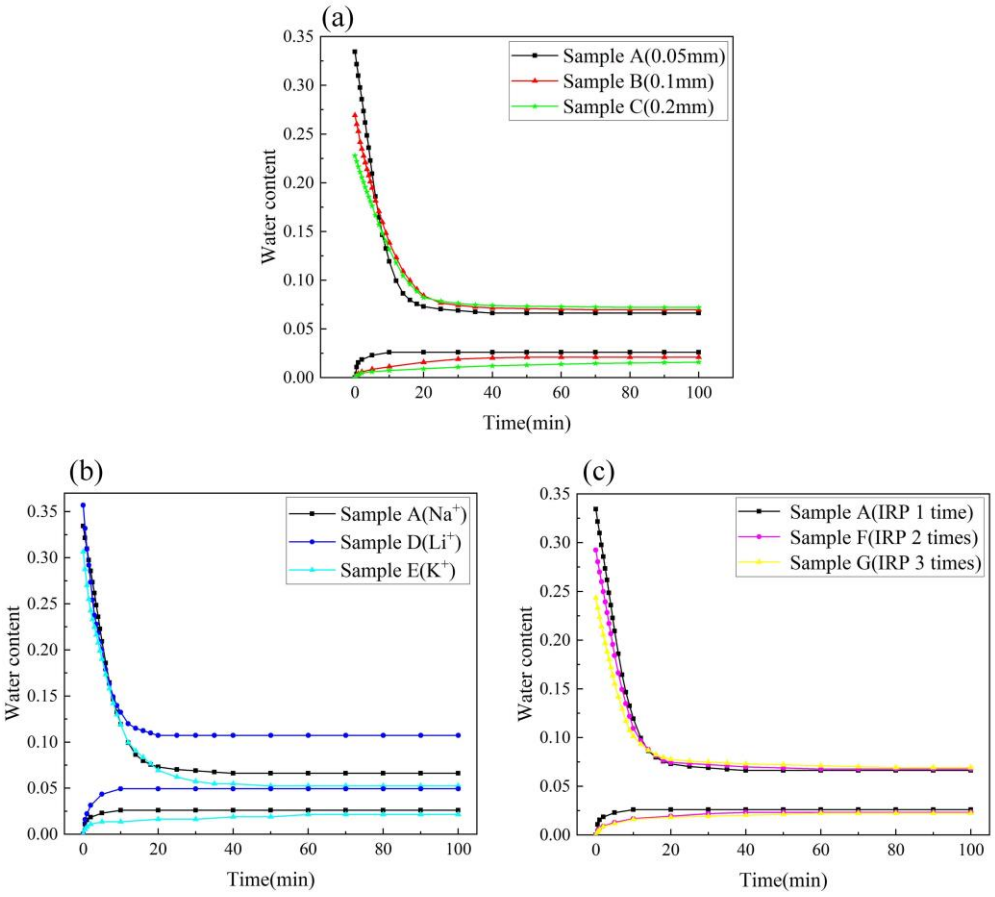

Fig. 7. Changes of water content of different samples during water absorption and desorption. (a) Water absorption and desorption progress of samples with different thickness. (b) Water absorption and desorption progress of samples with different cations. (c) Water absorption and desorption progress of samples with different IRP times.

Fig.7 shows the evolution of water content during water absorption and desorption for each sample. It can be seen from the curves that the total trend presents a quick drop for desorption and a slow rise for absorption, and then slowly reaching equilibrium position for all samples. Theoretically, the final equilibrium position, whether desorption or absorption, will reach the same value in the air. However, in fact there is an obvious gap between them for each sample, which is attributed to the insufficient exchange time. In terms of thickness (Fig.7 (a)), the sample with smaller

thickness shows a higher speed of water desorption and absorption. Because the thicker Nafion has a larger ion storage capacity, more palladium ions are exchanged during the immersion process and reduced to the surface during the IRP process, which would result in more compact surface electrode and block water molecules from coming in and out. The water content evolution of the samples with different cations was given in Fig.7 (b). In the first 10s, the downward trend of water content looks exactly the same for each sample and from 10 s to 30 s, water desorption of sample D becomes slower than sample A and E. Meanwhile, the water content of equilibrium position is shifted from 0.05 for sample K^+ to 0.12 for sample Li^+, which was decided by the ability of cations to bind water molecules. According to ion drag theory in solution, the binding water molecular capacity of the three cations meets the following order of $Li^+>Na^+>K^+$, which leads to the difference in the equilibrium water content among them. As for the upward trend of water content, the speed of water absorption also satisfies the order of $Li^+>Na^+>K^+$. For the reason of almost no water molecules inside sample after vacuum drying, the stronger the water binding capacity of the cation, the faster the cations absorb water and vice versa. Fig.7 (c) shows the water content evolution of the samples with different IRP times. The sample with less IRP times has the faster water absorption and desorption speed, which is also determined by the degree of surface electrode looseness. When the IRP times are increased, more Pd^+ will be deposited on IPMC surface and the surface electrode will become more compact. The water absorption and desorption characteristics of

different samples could cast a light on the characteristics of humidity response and results.

3.2 Humidity-capacitance response

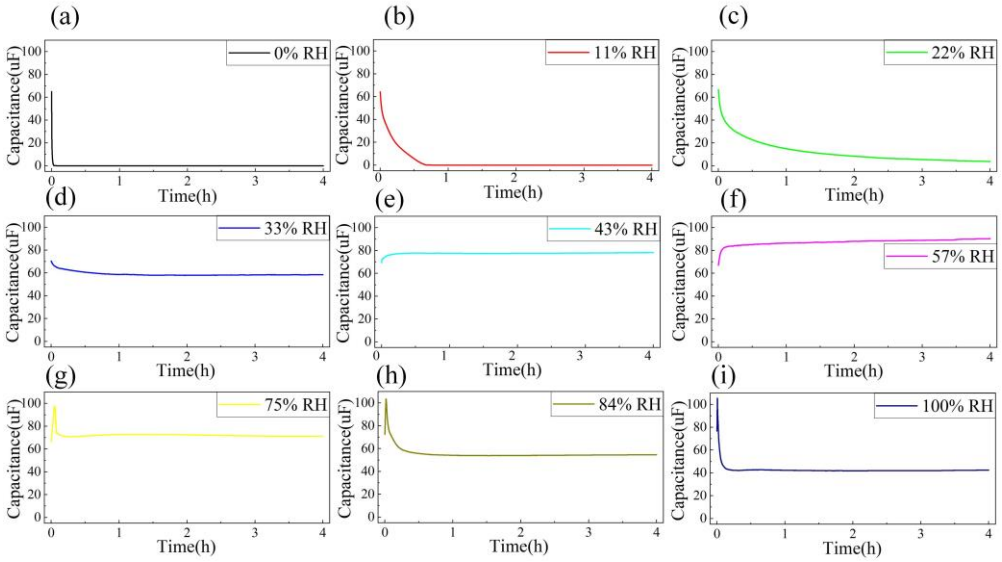

Fig. 8. Capacitance evolution of sample A under different humidity conditions. (a) Capacitance evolution of sample A at 0% RH. (b) Capacitance evolution of sample A at 11% RH. (c) Capacitance evolution of sample A at 22% RH. (d) Capacitance evolution of sample A at 33% RH. (e) Capacitance evolution of sample A at 43% RH. (f) Capacitance evolution of sample A at 57% RH. (g) Capacitance evolution of sample A at 75% RH. (h) Capacitance evolution of sample A at 84% RH. (i) Capacitance evolution of sample A at 100% RH.

The capacitance evolution was evaluated by transferring sample A from room humidity (40% RH) to a set of humidity levels as presented in Table 2. Sample A was placed in room humidity for about half an hour before being placed in other humidity levels. The test results are shown in Fig. 8. When the humidity set was less than or equal to 33% RH, the capacitance value presented a relatively quick downward trend

while a slowly upward trend would appear when the humidity set was between 43% RH and 57% RH separately. When the humidity set was higher than 60% RH, at first the capacitance quickly soared to a peak and then slowly decreased. At most humidity levels, capacitance achieved a stable value within half an hour, but it would take a longer time to stabilize at 22% RH.

The circularity and long-term stability of humidity capacitance sensing are shown in Figure 9. As shown in Fig. 9(a), the circularity was tested by sample G, the capacitance value during the humidity down process is slightly higher than that during the humidity up process. As shown in Fig. 9(b), the long-term stability was characterized by testing the capacitance value of sample A under 57% RH. It shows a relatively stable trend within 8 days, and the capacitance error rate is about 7%.

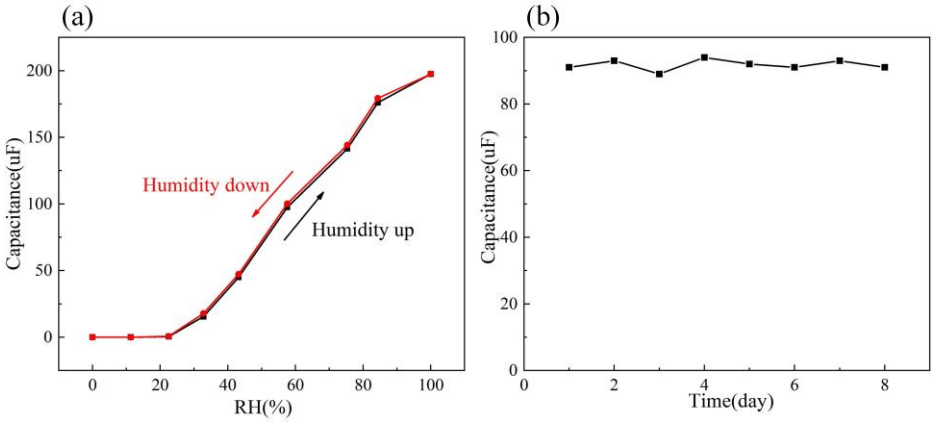

Fig. 9. (a)Circularity of sample G in humidity capacitance sensing. (b) Long-term stability of sample A under 57% RH.

We extracted the steady-state value of the capacitance response after 4 h from Fig.8, which were shown in Fig. 10 (a) (black line). Consistent with *Emad Esmaeli*'s experimental results, the capacitance value measured by the multimeter was close to 0 uF at 0% RH and 11% RH. One possible explanation is that the internal moisture

content of IPMC is too low to measure the capacitive reactance of IPMC at the inherent frequency (50 Hz) of the multimeter. With the increase in humidity, the steady-state capacitance value of sample A gradually climbs up, which results from the increased surface area and internal dielectric constant after hygroscopic expansion of IPMC. However, as the humidity increases further (higher than 60% RH), the steady-state capacitance value of sample A shows a downward trend, which is attributed to the looseness degree of the surface electrode. *K.Narimani* et al. [28] proposed a model to explain the above capacitance evolution. The surface electrode of IPMC presents intrinsic cracks, which will expand after water absorption, and then the surface electrode layer will be torn. Due to the weak connection force and expansion effect after water absorption among the loose electrode zones on the surface, cracks spread and scattered islands of small electrodes are formed. Therefore, the whole IPMC is divided into many small capacitors, and only a part of them can be measured by the multimeter so that the capacitance presents a downward trend.

Following the above procedure, the other samples in Tab.1 were also put into given humidity levels in Table 2 for 4 h, the steady-state capacitance value after 4 h of each sample were extracted and shown in Fig. 10. The effects of thickness on the steady value of capacitance response were evaluated by comparing sample A, B and C, which were shown in Fig. 10 (a). When the humidity level is less than 22% RH, the capacitance value of each sample is 0 μF. At 22% RH, it can be seen that sample A has a capacitance value of 2.4 μF, while sample B and sample C have capacitance values of nearly 0 μF. It indicates that a thinner sample has a better response at low

humidity level, which can be attributed to a higher water absorption capacity of sample A than sample B and C according to the test results in Fig. 7 (a). When the humidity level is between 22% and 57%, sample A has the highest steady value of capacitance, sample B takes the second place and sample C has the lowest steady value of capacitance. It is caused by the water absorption capacity of each sample. When the humidity level is higher than 57% RH, sample C has the highest steady value of capacitance while the other two samples show a downward trend. Meanwhile, it is worth noting that the capacitance values of sample C presents an approximate linear relation to humidity levels unlike sample A and B.

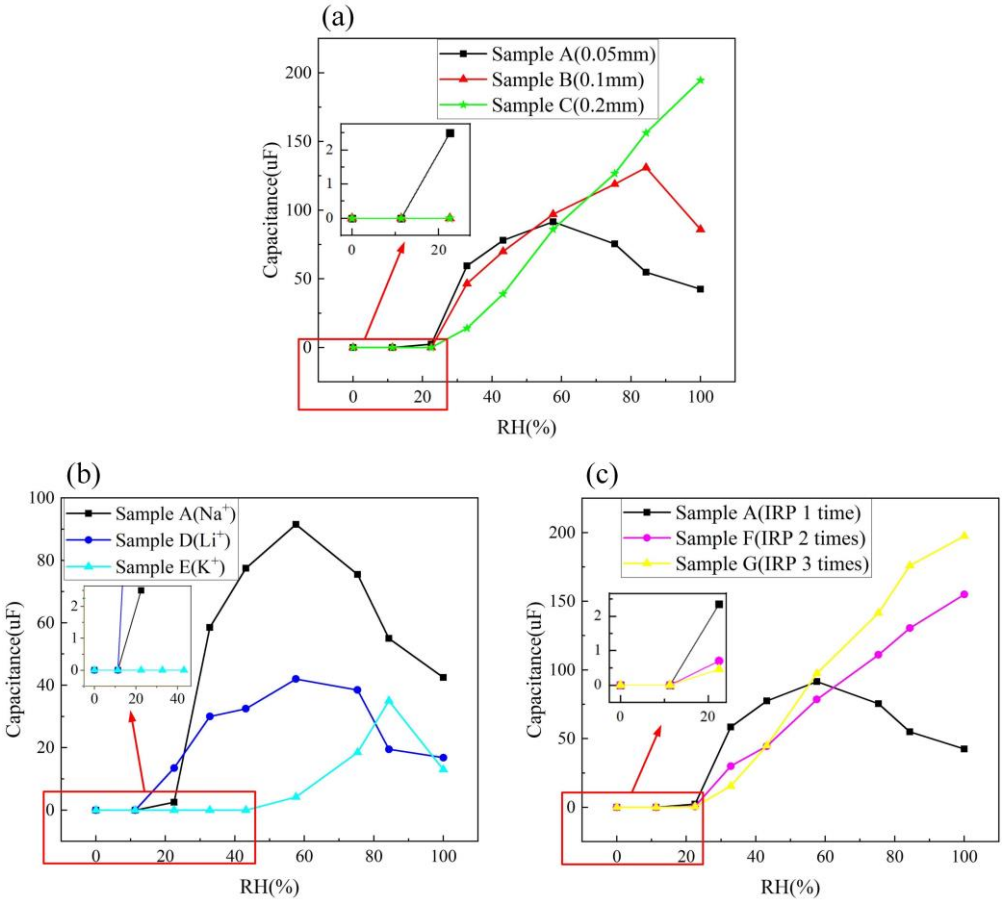

Fig. 10. Comparison of the steady value of capacitance response of each sample at different humidity. (a) The steady value of capacitance response of samples with different thickness at

different humidity. (b) The steady value of capacitance response of samples with different cations at different humidity. (c) The steady value of capacitance response of samples with different IRP times at different humidity.

By comparing sample group (A, D and E) and sample group (A, F and G), we further evaluate the effects of cations and IRP times on the steady value of the capacitance responses, as shown in Fig. 10 (b) and (c) respectively. In Fig. 10 (b), for each sample, the steady value of the capacitance response was 0 μF when the humidity level is lower than 22% RH. And at 22% RH, sample D has the largest capacitance value of 11 μF because of its best water absorption capacity. The steady value of the capacitance responses of sample D keeps 0 μF until the humidity level reaches 57% RH, which is related to its poor water absorption capacity. In Fig. 10 (c), it shows a similar rule that the sample with less IRP times has a higher steady value of capacitance responses at low humidity level due to its better water absorption capacity. And as the IRP times increase, the steady value of capacitance responses shows an upward trend as the humidity level increases. One reasonable explanation could be more IRP times causing higher electrode connection force and worse water absorption capacity.

In order to further investigate the characteristics of capacitance response, the response rate of all samples listed in Tab.1 were explored and calculated. Each sample was placed in 33% RH for 4 h to stabilize its capacitance value, then it was quickly placed in 57% RH environment and capacitance changes were recorded before sorting. The real-time capacitance value of IPMC is defined as C, the steady-state capacitance

value at 33% RH is $C_{33\%RH}$ and the steady-state capacitance value at 57% RH is $C_{57\%RH}$. The response degree is defined as ω, the calculation formula of which is as follow.

$$\omega = \frac{C - C_{33\%RH}}{C_{57\%RH} - C_{33\%RH}} \tag{2}$$

The evolution of ω for different samples shows that the response speed of different samples is consistent with their water absorption capacity, as shown in Fig. 10. As the thickness (Fig. 11 (a)), cation radius (Fig. 11 (b)) and IRP times (Fig. 11 (c)) of the sample increase, the response speed becomes slower.

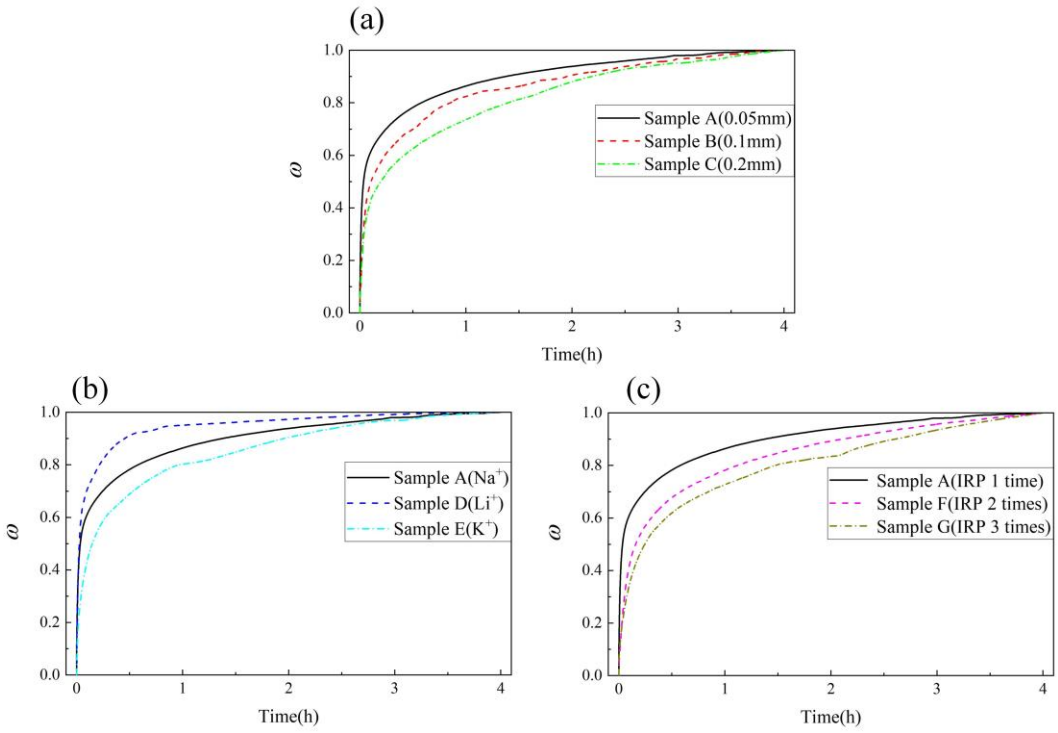

Fig. 11. Comparison of response degree of each sample from 33% RH to 57% RH. (a) The evolution of response degree of samples with different thickness. (b) The evolution of response degree of samples with different cations. (c) The evolution of response degree of samples with different IRP times.

As for the humidity perception, more concerns were focused on the sensitivity at low humidity levels. Therefore, the sensitivity of each sample when the humidity level is less than or equal to 22% RH was calculated and listed in Table 3. It can be seen that most samples nearly have no sensing ability while sample D has the highest sensitivity of 61.36 μF.

Table 3. Sensitivity of each sample between 0%RH and 22%RH

Sample	A	B	C	D	E	F	G
Sensitivity(μF)	11.36	0	0	61.36	0	3.18	2.09

From the above results, sample D shows the highest response speed and the highest sensitivity at low humidity level. The only drawback of it is that its steady value of capacitance responses shows a downward trend at high humidity level, but that can be improved by increasing the thickness or IRP times.

3.3 Humidity-surface resistance response

Considering that the surface resistance response is only related to the impedance characteristics of the surface electrode and has little relation to the internal state and thickness of IPMC, we selected sample A, F and G to evaluate the effects of IRP times on the surface resistance response.

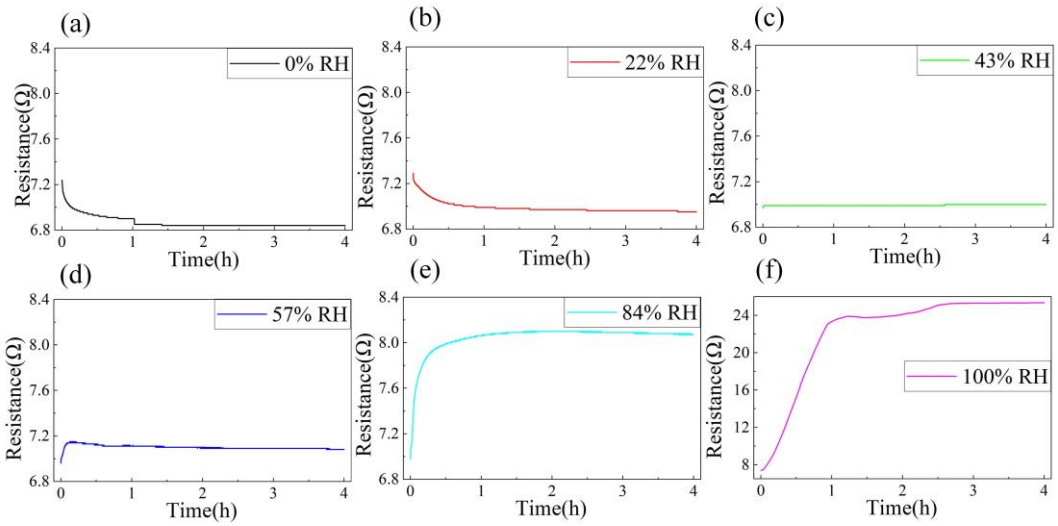

Fig. 12. Resistance evolution of sample G under different humidity conditions. (a) Resistance evolution of sample G at 0% RH. (b) Resistance evolution of sample G at 22% RH. (c) Resistance evolution of sample G at 43% RH. (d) Resistance evolution of sample G at 57% RH. (e) Resistance evolution of sample G at 84% RH. (f) Resistance evolution of sample G at 100% RH.

The surface resistance evolution was evaluated by transferring sample G from room humidity (40% RH) to 0% RH, 22% RH, 43% RH, 57% RH, 84% RH and 100% RH, respectively, which were selected from Table 2. Sample G was placed in room humidity for about 0.5 h before being placed in other humidity levels. The test results are shown in Fig. 12. As the humidity level increases, the steady value of surface resistance response of sample G increases as well. And it takes a longer time to reach stable state as the humidity gradient becomes greater. For example, it takes 20 min for sample G to stabilize at 57% RH, while it takes about 3 h to stabilize at 100% RH.

The circularity and long-term stability of humidity resistance sensing are shown in Figure 13. As shown in Fig. 13(a), the circularity was tested by sample G, the resistance value during the humidity down process is slightly higher than that during

the humidity up process. As shown in Fig. 13(b), the long-term stability was characterized by testing the resistance value of sample A under 57% RH. It shows a relatively stable trend within 8 days, and the capacitance error rate is about 5.3%.

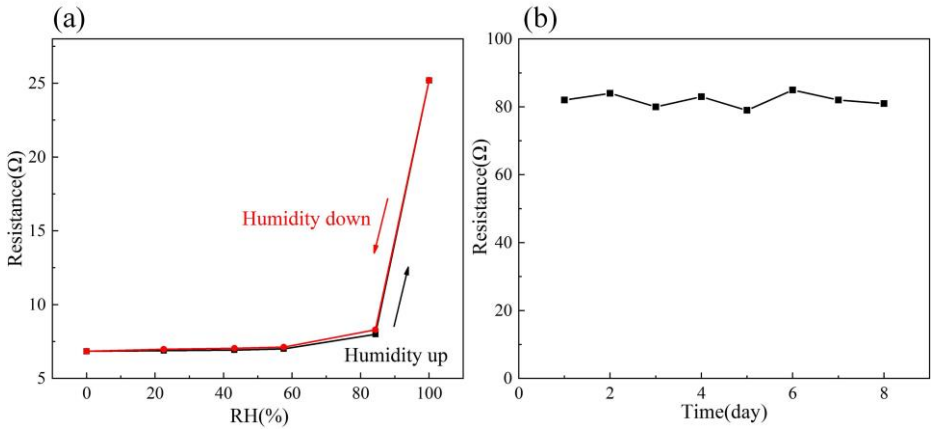

Fig. 13. (a)Circularity of sample G in humidity resistance sensing. (b) Long-term stability of sample A under 57% RH.

Similarly, sample A and F were placed in the given humidity levels for 4 h to test their surface resistance evolution. The steady-state surface resistance value after 4 h of sample A, F, and G were extracted and shown in Fig. 14. First of all, the steady-state surface resistance value of each sample shows an upward trend as the humidity level increases. *A.Punning* et al. [29] proposed a model to explain it. The surface electrode of IPMC is separated and there are cracks between the electrode blocks. The surface resistance will increase along with the size of the cracks. When the humidity level rises, IPMC will expand by absorbing water and the size of the cracks will get large accordingly so that the surface resistance will increase. Our previous work also confirmed this point. The surface electrode change of IPMC during water desorption were observed by a confocal microscope [30]. The size of the cracks showed a downward trend as the water content decreased. Meanwhile, it can be intuitively seen

that the sample with less IRP times has a higher steady-state surface resistance value and sensitivity, which is determined by surface resistance and water absorption capacity of each sample.

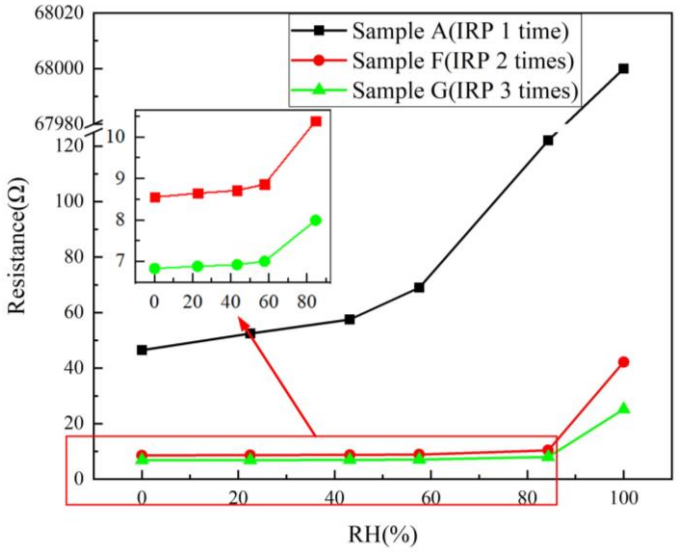

Fig. 14. Resistance response of samples with different IRP times at different humidity

As for the sensitivity, each sample has a higher sensitivity at higher humidity levels. For example, when the humidity is lower than 84% RH, the sensitivity is relatively stable, when the humidity is higher than 84% RH, the sensitivity rises sharply, which should be related to the water content of the sample under certain humidity. For this reason, we measured the water content of sample G at given humidity levels. Sample G was placed in different humidity bottles for 12 h to allow its mass to reach stable state. Formula (1) was used to calculate the equilibrium water content of sample G at certain humidity level and the calculating results were shown in Fig. 15. It can be seen that the increase rate of water content becomes higher as the humidity level increase, which is consistent with the change rule of sensitivity. In addition, it is obvious that the sample with fewer IRP times has a higher sensitivity.

Because the sensitivity is relatively stable when the humidity is lower than 84% RH, we calculated the sensitivity between 0% RH and 84% RH, sample A has a sensitivity of 88.9 Ω, while sample F and G have the sensitivity of 2.2 Ω and 1.4 Ω.

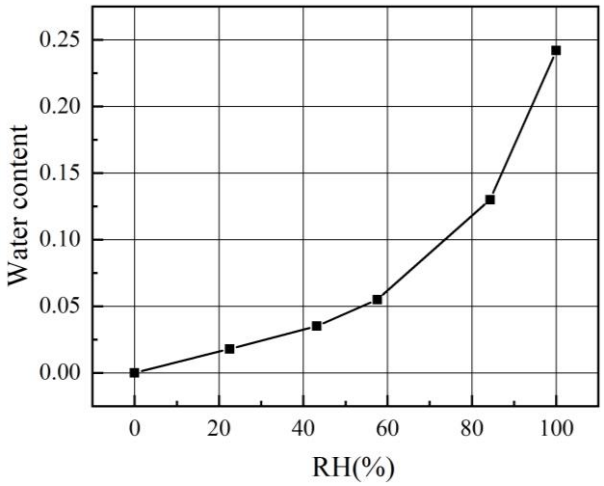

Fig. 15. Equilibrium water content of sample G under given humidity level

In order to further investigate the response characteristics of surface resistance, the response rate of sample A, F, and G were explored and calculated. Each sample was placed in 57% RH for 4 h to stabilize its surface resistance, then it was quickly placed in 0% RH and the surface resistance changes were recorded before sorting. The real-time surface resistance value is defined as r, the stable surface resistance value at 0% RH is R and the stable capacitance value at 57% RH is $R_{57\%RH}$. The response degree is defined as η and the calculation formula can be expressed as follow.

$$\eta = \frac{R_{57\%RH} - r}{R_{57\%RH} - R} \tag{3}$$

The evolution of η for different samples shows that the response speed of different samples is also consistent with their water absorption capacity, as shown in

Fig. 16. As the IRP times of the sample increase, the response speed will become slower.

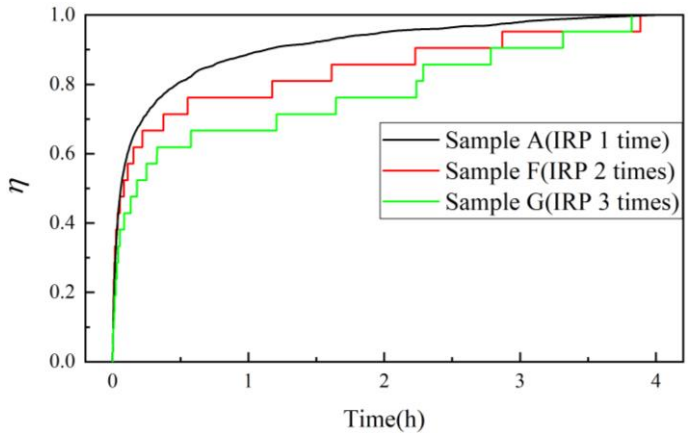

Fig. 16 .Comparison of response degree of each sample from RH 57% to RH 0%

Through the above research, it can be concluded that the surface resistance response can realize sensing of the full humidity range while the capacitance response can only sense humidity higher than 22% RH. And we can obtain higher sensitivity and response speed by reducing the IRP times of the sample.

3.4 Humidity-ionic electrical response

The voltage evolution was evaluated by switching sample B to given humidity levels after stabilized at 57% RH. The test results are shown in Fig. 17. First of all, the voltage shows an upward trend from 57% RH to higher humidity levels while it shows a downward trend from 57% RH to lower humidity levels. Because when the humidity level is switched from 57% RH to a higher one, the ion concentration on the hygroscopic side of IPMC will decrease by absorbing water, thus the cations will move from the fixed surface to the hygroscopic surface, and vice versa. In addition, it can also be concluded that the voltage amplitude will rise along with the humidity

gradient. Since the humidity gradient increases, IPMC will absorb or lose more water so that a larger voltage amplitude will generate. In terms of response time, the ionic electrical response shows an extremely short time of less than 0.5 s compared with the capacitance and surface resistance response.

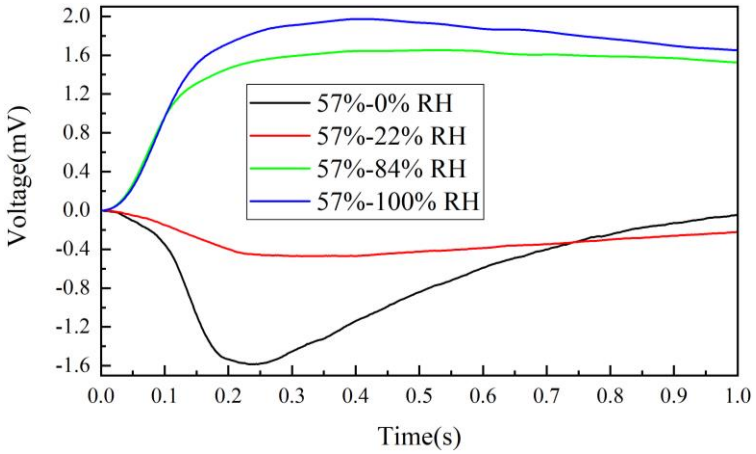

Fig. 17. Voltage change of sample B from 57% RH to other humidity levels.

As for humidity-ionic electrical response, the results display a vector feature from decrease to increase for the same humidity levels, which cannot be characterized by traditional circularity. Therefore, we tested the humidity absorption and desorption response of sample G as shown in Fig. 4(a). The polarity of the voltage response during humidity absorption and desorption process is opposite, and the absolute value of the moisture absorption response is slightly larger. It is worth noting that for the case of 0% RH-57% RH, the voltage response is almost approach to 0 V. This is ascribed to the slow process of absorbing water after fully water loss, which has been observed in our previous work [2]. As shown in Fig. 4(b), The long-term stability was characterized by testing the peak voltage value of sample A from 57% RH to 100% RH. It shows a relatively stable trend within 8 days, and the voltage error rate is about 4.7%.

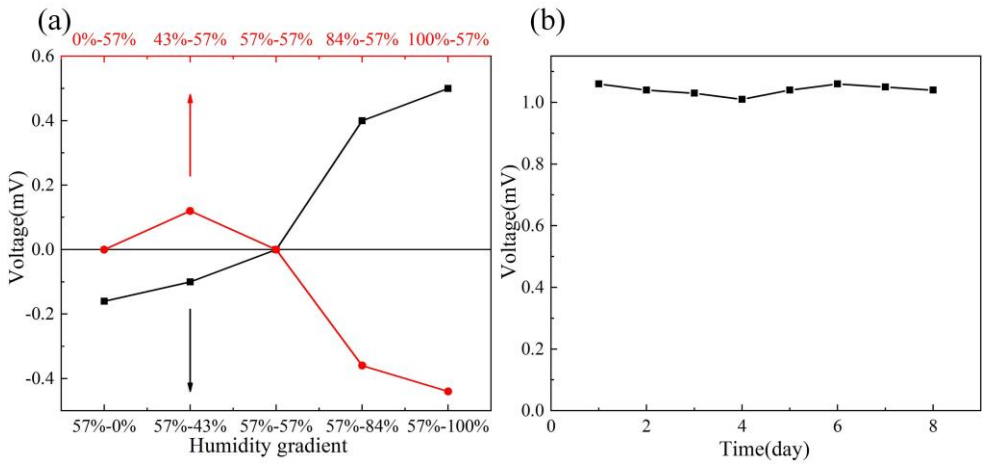

Fig. 18. (a)Circularity of sample G in humidity ionic electrical response. (b) Long-term stability of the peak voltage of sample A from 57% RH to 100% RH.

The voltage maximum of each sample in Tab.1 was extracted as the ionic electrical response value and shown in Fig.19. The effects of thickness on the ionic electrical response value were evaluated by comparing sample A, B and C, which was shown in Fig. 19 (a). When the thickness of the samples increases from 0.05 mm to 0.1 mm, the ionic electrical response value increases apparently, while when the thickness further increases to 0.2 mm, the ionic electrical response value drops to a very low level. One possible reason could be that ionic electrical response is the result of the comprehensive action of the number of cations and the water absorption capacity. As the thickness of the sample increases, the number of cations contained in the inner layer will increase subsequently but the water absorption capacity of the sample will decrease according to Fig. 7. Compared with sample A, the influence of increasing number of cations of sample B is greater than the influence caused by the decrease of the water absorption capacity, so the ionic electrical response value increases. As for sample C, although the number of the cations increases further, the

influence of its water absorption capacity is much greater, so the ionic electrical response value decreases. By comparing sample group (A, D and E) and sample group (A, F and G), we further evaluate the effects of cations and IRP times on the ionic electrical response, as shown in Fig. 19 (b) and (c) respectively. In Fig. 19 (b), it can be clearly seen that the ionic electrical response value of samples with different cations is consistent with their water absorption capacity. Sample D has the highest electrical response value that is 10-fold higher than sample A and E. In Fig. 19 (c), the ionic electrical response value of samples with different IRP times also corresponds with their water absorption capacity. As the IRP times increase, the ionic electrical response value of samples decreases subsequently.

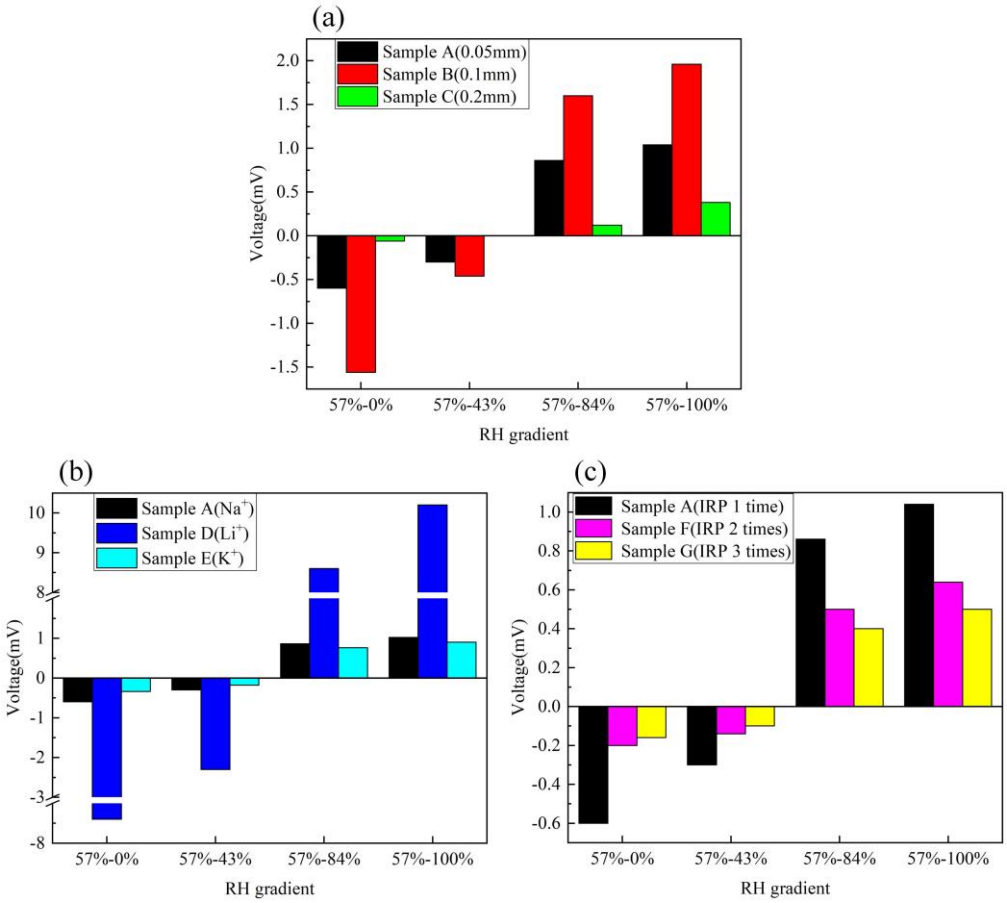

Fig. 19. Comparison of voltage response of each sample at different RH gradient. (a) Voltage

response of samples with different thickness at different RH gradients. (b) Voltage response of samples with different cations at different RH gradients. (c) Voltage response of samples with different IRP times at different RH gradients.

As for the sensitivity, it is also different from the capacitance and resistance. We defined the sensitivity as the ratio of the peak voltage to the difference of humidity levels, and the sensitivity of each sample from 57% RH to 100% RH was calculated and shown in Table 4. The sensitivity of each sample is still related to the moisture absorption capacity, sample D shows a sensitivity of 23.7 mV, which is far superior to other samples.

Table 4. Sensitivity of each sample from 57%RH and 100%RH

Sample	A	B	C	D	E	F	G
Sensitivity(mV)	2.42	4.56	0.88	23.7	2.09	1.49	1.16

In order to further investigate the characteristics of ionic electrical response, the response time and rate of each sample was explored and calculated. The ionic electrical response process from 57% RH to 100% RH of each sample was studied. The ionic electrical response amplitude from 57% RH to 100% RH is defined as ΔV, and the response time is defined as t, then the response rate can be defined as $\Delta V/t$. The response time and response rate of each sample are listed in Table 5. It can be concluded that the response time is related to the water absorption capacity of the sample. As the water absorption capacity increases, the response time will rise. The response rate is determined by the response time and response amplitude, and sample D has the fastest response rate of 6 mV/s.

Table 5. The response time and response rate of each sample

Sample	A	B	C	D	E	F	G
t(s)	0.5	0.4	0.32	1.7	0.2	0.3	0.2
$\Delta V/t$(mV/s)	2.08	4.9	1.19	6	4.5	2.13	2.5

Through the above research, it can be concluded that the ionic electrical response has an extremely short response time of less than 0.5 s, which is much shorter than that of capacitance and surface resistance response. With the increase of the water absorption capacity of the samples, the ionic electrical response value will become larger but the response time will be longer.

4 Conclusion

In this work, the humidity sensing performance of IPMC is systematically investigated through capacitance, resistance and ionic electrical response for the first time. Considering the change of the thickness, cations and impregnation-reduction plating (IRP) times, a set of humidity sensing tests by static and dynamic humidity platform were performed for each specific parameter. It is found that capacitance and resistance can sense static humidity, while ionic electrical response can only sense dynamic change of humidity. The humidity response characteristics are closely related to the water absorption capacity of the sample. Samples with stronger water absorption capacity will generate greater humidity response. In addition, we also found that the capacitance response cannot respond to all the humidity levels (only working from 22% RH to 100% RH), and the ionic electrical response is much quicker (less than 0.5 s) than the capacitance and resistance response (several hours). The obtained results of IPMC sensors could be feasible for humidity sensing in

practical applications like robotic, biomimetic, etc. In the future work, the empirical findings obtained in the experiment will be applied to humidity detection, and a multiparameter humidity sensor will also be developed.

Acknowledgements

This research was supported by the financial support from the National Natural Science Foundation of China (51975184), the National Key Research and Development Program of China (2020YFB1312900), the Fundamental Research Funds for the Central Universities (B210202124 and PA2020GDSK0074) and China Postdoctoral Science Foundation funded project (2019M661706). The authors gratefully acknowledge the supports.

References

[1] Annabestani M, Naghavi N, Maymandi-Nejad M. From modeling to implementation of a method for restraining back relaxation in ionic polymer–metal composite soft actuators. Journal of intelligent material systems and structures. 2018, 29 (15), 3124-3135.

[2] Bashir M, Rajendran P. A review on electroactive polymers development for aerospace applications. Journal of Intelligent Material Systems and Structures. 2018, 29(19), 3681-3695.

[3] Shahinpoor M, Kim K J. Ionic polymer–metal composites: III. Modeling and simulation as biomimetic sensors, actuators, transducers, and artificial muscles. Smart materials and structures. 2004, 13 (6), 1362.

[4] Bhandari B, Lee G.-Y, Ahn S H. A review on IPMC material as actuators and sensors: fabrications, characteristics and applications. International journal of precision engineering and manufacturing. 2012, 13 (1), 141-163.

[5] Wang Y. Chen H. Wang Y, Zhu Z, Li D. Effect of dehydration on the mechanical and physicochemical properties of gold-and palladium-ionomeric polymer-metal composite (IPMC) actuators. Electrochimica Acta. 2014, 129, 450-458.

[6] Wang Y, Zhu Z, Liu J, Chang L, Chen H. Effects of surface roughening of Nafion 117 on the mechanical and physicochemical properties of ionic polymer–metal composite (IPMC) actuators. Smart Materials and Structures. 2016, 25 (8), 085012.

[7] Yang L, Zhang D, Wang H, Zhang X. Actuation Modeling of Ionic–Polymer Metal Composite Actuators Using Micromechanics Approach. Advanced Engineering Materials. 2020, 22(12), 2000537.

[8] Jung K, Nam J, Choi H. Investigations on actuation characteristics of IPMC artificial muscle actuator. Sensors & Actuators A Physical. 2003, 107 (2), 183-192.

[9] Punning, A.; Kruusmaa, M.; Aabloo, A., A self-sensing ion conducting polymer metal composite (IPMC) actuator. Sensors & Actuators A Physical 2007, 136 (2), 656-664.

[10] Qaviandam Z, Naghavi N, Safaie J. A New Approach to Improve IPMC Performance for Sensing Dynamic Deflection: Sensor Biasing. IEEE Sensors Journal. 2020, PP(99), 1-1.

[11] Bonomo C, Fortuna L, Giannone P, Graziani S. A method to characterize the deformation of an IPMC sensing membrane. Sensors & Actuators A Physical. 2005, 123, 146-154.

[12] Liu H, Xiong K, Bian K, Zhu K. Experimental study and electromechanical model analysis of the nonlinear deformation behavior of IPMC actuators. Acta Mechanica Sinica. 2017, 33 (2), 382-393.

[13] Gudarzi M, Smolinski P, Wang Q M. Compression and shear mode ionic polymer-metal composite (IPMC) pressure sensors. Sensors and Actuators A Physical. 2017, 260, 99-111.

[14] Gudarzi M, Smolinski P, Wang Q M. Bending mode ionic polymer-metal composite (IPMC) pressure sensors. Measurement. 2017, 103, 250-257.

[15] Topcu G, Guner T, Demir M M. Pressure Sensors Based on IPMC Actuator. Ionic Polymer Metal Composites for Sensors and Actuators, Springer. 2019, pp, 161-182.

[16] Lee J H, Nam J D, Choi H, Jung K, Jeon J W, Lee Y K, Kim K J, Tak Y. Water uptake and migration effects of electroactive ion-exchange polymer metal composite (IPMC) actuator. Sensors & Actuators A Physical. 2005, 118 (1), 98-106.

[17] Shoji E, Hirayama D. Effects of humidity on the performance of ionic polymer-metal composite actuators: experimental study of the back-relaxation of actuators. Journal of Physical Chemistry B. 2007, 111 (41), 11915-11920.

[18] Brunetto P, Fortuna L, Giannone P, Graziani S, Strazzeri S. Characterization of the Temperature and Humidity Influence on Ionic Polymer-Metal Composites as Sensors. IEEE Transactions on Instrumentation & Measurement. 2011, 60 (8), 2951-2959.

[19] Zhu Z, Horiuchi T, Kruusamäe K, Chang L, Asaka K. Influence of ambient humidity on the voltage response of ionic polymer–metal composite sensor. The Journal of Physical Chemistry B. 2016**,** 120 (12), 3215-3225.

[20] Zhu Z, Horiuchi T, Takagi K, Takeda J, Chang L, Asaka K. Effects of cation on electrical responses of ionic polymer-metal composite sensors at various ambient humidities. Journal of Applied Physics. 2016, 120 (8), 084906.

[21] Ru J, Zhu Z, Wang Y. Chen H, Bian C, Luo B, Li D. A moisture and electric coupling stimulated ionic polymer-metal composite actuator with controllable deformation behavior. Smart Materials and Structures. 2018, 27, 02LT01.

[22] Esmaeli E, Ganjian M, Rastegar H, Kolahdouz M, Kolahdouz Z, Zhang G Q. Humidity sensor based on the ionic polymer metal composite. Sensors and Actuators B Chemical. 2017, 247, 498-504.

[23] Beigi F, Mousavi M S S, Manteghi F, Kolahdouz M. Doped nafion-layered double hydroxide nanoparticles as a modified ionic polymer metal composite sheet for a high-responsive humidity sensor. Applied Clay Science. 2018, 166, 131-136.

[24] Hofmann D W, Kuleshova L, D'Aguanno B, Di Noto V, Negro E, Conti F, Vittadello M. Investigation of water structure in Nafion membranes by infrared spectroscopy and molecular dynamics simulation. The Journal of Physical Chemistry B. 2009, 113 (3), 632-639.

[25] Jiang B, Yu L, Wu L, Mu D, Liu L, Xi J, Qiu X. Insights into the impact of the nafion membrane pretreatment process on vanadium flow battery performance. ACS Applied Materials & Interfaces. 2016, 8 (19), 12228-12238.

[26] Hosokawa H, Funasako Y, Mochida T. Colorimetric Solvent Indicators Based on Nafion Membranes Incorporating Nickel (II)-Chelate Complexes. Chemistry-A European Journal. 2014, 20 (46), 15014-15020.

[27] Greenspan L. Humidity fixed points of binary saturated aqueous solutions. Journal of research of the national bureau of standards. 1977, 81 (1), 89-96.

[28] Narimani K, Nayeri F D, Kolahdouz M, Ebrahimi P. Fabrication, modeling and simulation of high sensitivity capacitive humidity sensors based on ZnO nanorods. Sensors and Actuators B Chemical. 2016, 224, 338-343.

[29] Punning A, Kruusmaa M, Aabloo A. Surface resistance experiments with IPMC sensors and actuators. Sensors and Actuators A Physical. 2007, 133 (1), 200-209.

[30] Wang Y, Chen H, Wang Y, Zhu Z, Li D. Effect of dehydration on the Mechanical and Electrochemical Properties of Gold- and Palladium- Ionomeric Polymer-Metal Composite (IPMC) actuators. Electrochimica Acta. 2014, 129, 450-458.

[31] Wang Y, Wang J, Hao M, Li B, Zhu Z, Gou X, Li L. Rapid preparation of a Nafion/Ag NW composite film and its humidity sensing effect. RSC Advances. 2020, 10, 27447.